Applied Geochemistry 152 (2023) 105649

Contents lists available at ScienceDirect

Applied Geochemistry

journal homepage: www.elsevier.com/locate/apgeochem

The mechanisms and microstructures of passive atmospheric CO_2 mineralisation with slag at ambient conditions

John M. MacDonald [a,*], Faisal W.K. Khudhur [a], Ruth Carter [a], Ben Plomer [a], Claire Wilson [b], Charlotte Slaymark [a]

[a] School of Geographical and Earth Sciences, University of Glasgow, Glasgow, G12 8QQ, UK
[b] School of Chemistry, University of Glasgow, Glasgow, G12 8QQ, UK

ARTICLE INFO

Editorial Handling by: Thomas Gimmi

Keywords:
CO_2 mineralisation
Waste management
Slag
Microstructures

ABSTRACT

Removal of CO_2 already in the Earth's atmosphere through CO_2 mineralisation with alkaline waste materials such as steel slag is one approach to mitigate the effects of anthropogenically-induced climate change. However, the microstructures produced during passive carbonation of slag are not well known. Here we use Scanning Electron Microscopy imaging and chemical mapping, X-Ray diffraction and stable isotopes ($\delta^{13}C$ and $\delta^{18}O$) to show that ingassed and hydroxylated atmospheric CO_2 reacts with Ca leached from slag to precipitate calcite directly on the slag surface. Precipitated calcite crystal morphologies vary, ranging from bladed and acicular crystals to layered deposits of micron-scale equant crystals. The variable morphology and extent of calcite precipitation documented is linked to a combination of internal (i.e. microstructural properties of the slag itself) and external (environmental conditions) factors. This work shows that atmospheric CO_2 can be drawn down and mineralised passively by the slag at ambient conditions as part of the slag valorisation and reutilisation process.

1. Introduction

Removal of CO_2 already in the Earth's atmosphere through CO_2 mineralisation (Carbon Capture and Storage by Mineralisation (CCSM)) with alkaline materials is one approach to mitigate the effects of anthropogenically-induced climate change (Renforth, 2019). One such alkaline material is steel slag – a by-product from steel manufacture. Composed mainly of calcium-silicate mineral phases (e.g. Pullin et al., 2019), experimental studies have shown its potential for capturing atmospheric CO_2 by mineralisation (e.g. Huijgen et al., 2005). ~0.5 Gt of steelmaking slag is produced globally every year (USGS, 2018) and this could potentially reach ~2nullGtnullyr^{-1} by the end of the century (Renforth, 2019), in addition to an unquantified but undoubtedly large volume of legacy slag, stockpiled or dumped from historical steelmaking. Renforth (2019) calculated that steel slag could capture ~370–400 kg CO_2 per tonne of slag, depending on the type of slag. This rises to ~550–600 kg CO_2 per tonne of slag if carbonation is enhanced through experimental variation of reaction-influencing parameters. Modelling indicates that steel slag has the potential to capture ~150–250 Mt CO_2 yr^{-1} now, and ~320–870 Mt CO_2 yr^{-1} by 2100 (Renforth, 2019). This modelling shows that slag can play an important role in a mix of technologies to remove anthropogenically-produced CO_2 from the atmosphere. Utilizing slag in CO_2 mineralisation is particularly attractive since it can capture CO_2 emitted from a point source (i.e., a single location from which pollutants are released), therefore reducing the need for CO_2 and slag transportation (Kirchofer et al., 2013). Additionally, slag is widely used in construction applications. Netinger-Grubeša et al. (2016) noted that around 24% of blast furnace slag is used in construction application. For steel slag, the capacity of its utilization varies in different countries. In Japan, EU, and USA, slag utilization exceeds 75%, mostly in road construction, cement production and other civil engineering applications (Guo et al., 2018). Previous research showed that slag carbonation improved the mechanical properties of slag thereby enhancing its applicability as a construction material (Salman et al., 2014).

The CO_2 mineralisation process involves breakdown of slag minerals in dissolution and reprecipitation reactions (e.g. Mayes et al., 2018; Pullin et al., 2019). 'Fresh' (i.e. cooled after removal from the steelmaking furnace) slag minerals such as larnite (Ca_2SiO_4) undergo dissolution liberating Ca into solution (eq. (1)). The solution is alkaline due to hydroxide formation as part of the dissolution and this promotes CO_2 ingassing; the CO_2 reacts with water to produce bicarbonate (eq. (2))

* Corresponding author.
E-mail address: john.macdonald.3@glasgow.ac.uk (J.M. MacDonald).

https://doi.org/10.1016/j.apgeochem.2023.105649
Received 14 December 2022; Received in revised form 22 March 2023; Accepted 28 March 2023
Available online 31 March 2023

which reacts with the dissolved Ca to precipitate solid calcite (eq. (3)) (e.g. Mayes et al., 2018; Pullin et al., 2019).

$$Ca_2SiO_4 + 4H_2O \rightarrow 2Ca^{2+} + H_4SiO_4 + 4OH^- \quad (1)$$

$$CO_{2(g)} \leftrightarrow CO_{2(aq)} + H_2O \leftrightarrow HCO_{3(aq)}^- + H^+ \quad (2)$$

$$Ca^{2+} + 2HCO_{3(aq)}^- \leftrightarrow CaCO_{3(s)} + H_2O + CO_{2(aq)} \quad (3)$$

This suite of reactions has led to interest in slag as a material to mineralise CO_2. Various studies have sought to determine the optimum external environmental factors such as temperature, pCO_2 and humidity, as well as grain size, for maximising CO_2 mineralisation (enhanced carbonation, e.g. Baciocchi et al., 2009; Huijgen et al., 2005; Santos et al., 2013; van Zomeren et al., 2011). Typically, these studies ground up slag samples into fine powders and carbonated them in aqueous suspensions, varying particle size, temperature, pCO_2, reaction time, and batch reactor design (Baciocchi et al., 2009; Chang et al., 2012, 2013; Eloneva et al., 2008b; Huijgen et al., 2005; Santos et al., 2013; Yu and Wang, 2011); all studies found that finely ground slag in an aqueous suspension held at temperatures and CO_2 pressures well above Earth surface conditions maximised CO_2 capture.

Steel slag will also *passively* react with atmospheric CO_2 and store it as solid calcite via equations 1-3 – without any human intervention to enhance the reaction conditions. This passive carbonation has been documented at a site in Consett, North East England, where calcite has precipitated in a stream draining a legacy slag heap (Mayes et al., 2018; Pullin et al., 2019; Renforth et al., 2009). Slag and other waste from the former Consett Iron and Steel Works was dumped in the valley of the Howden Burn (a stream), and the water percolating through the slag resulted in dissolution and mobilisation of Ca^{2+} and OH^- from the slag. The high relief of the site is relatively unusual for slag heap locations, and resulted in calcite precipitation downstream from the slag heap. On emergence from the base of the slag heap, this hyperalkaline solution ingassed and hydroxylated atmospheric CO_2 precipitating calcite tufa barrages downstream. Given most slag heaps are not on top of hills with streams draining them, but are instead in low-relief areas often at the coast (Riley et al., 2020), CO_2 mineralisation is likely to more commonly occur directly on the slag surface, as opposed to ex-situ downstream as documented at Consett. Calcite coatings on the surface of slag pieces were noted by Khudhur et al. (2022b) and Hobson et al. (2017).

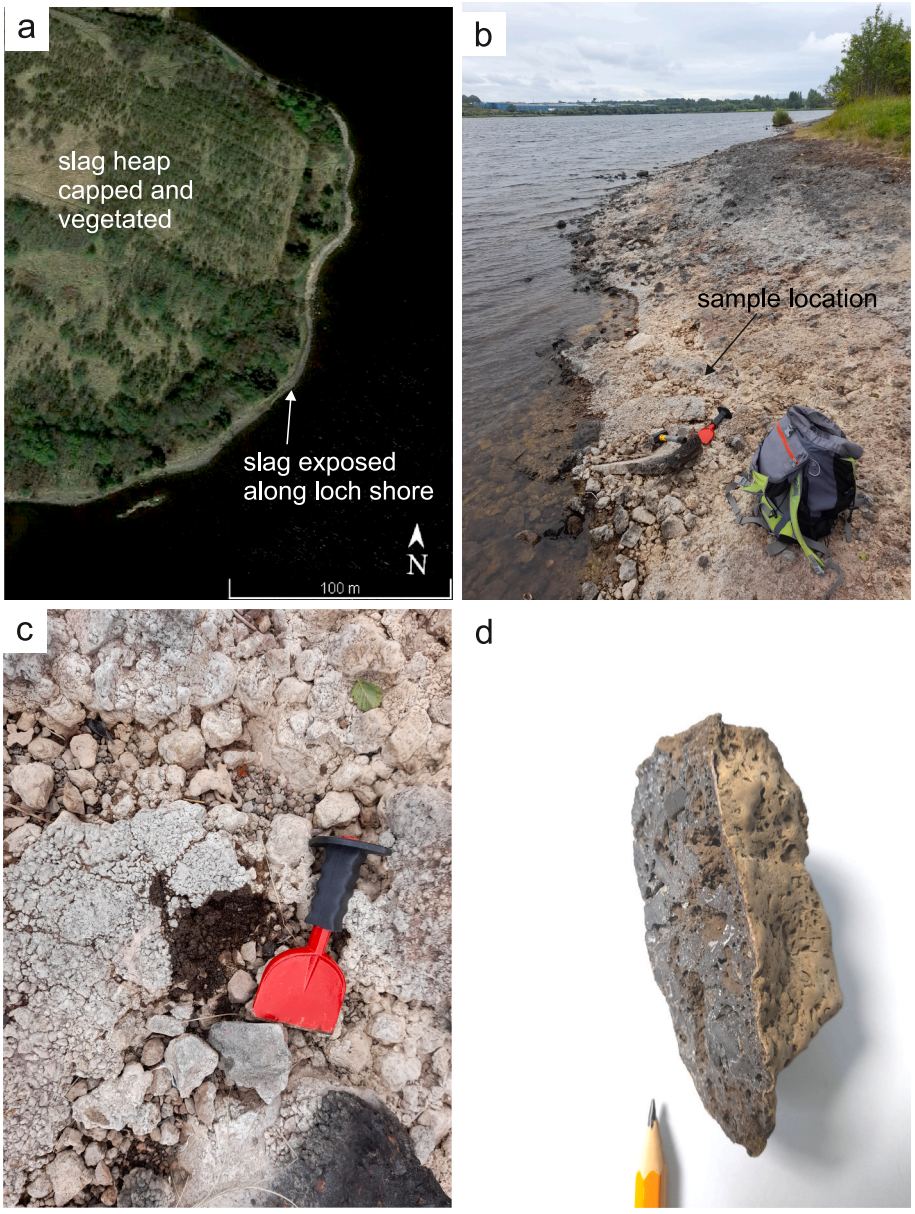

Fig. 1. a) satellite image of study site showing area of slag and adjacent loch; b) field photograph showing slag exposed on the loch shore (rucksack ~50 cm high for scale); c) field photograph showing slag on loch shore with distinctive white coating representing carbonation (15 cm long chisel for scale); d) photograph of cut section of collected slag sample showing fresh slag (dark grey colour) and narrow zone of creamy brown-coloured mineralised CO_2 on outer surface (1 cm pencil nib for scale).

The microstructures produced during passive carbonation of slag are not well known. However, pilot observation, together with examples from literature (Hobson et al., 2017; Khudhur et al., 2022b) indicate they may vary significantly, with variation driven by a range of factors. In this contribution, we use electron microscope imaging and chemical mapping to start to address these questions by documenting the microstructure of calcite precipitated directly on slag surfaces, the microstructure of the slag itself, and to highlight the formation mechanisms of the precipitated calcite.

2. Materials and methods

The case study site for this work was the former Glengarnock Steelworks in North Ayrshire, Scotland. A representative sample of slag (~1 kg) was taken for analysis from a slag deposit located on the north-western shore of a lake, Kilbirnie Loch (Fig. 1a). Historical map evidence indicates slag was dumped here from the 1940s until steelworks closure in 1978 (e.g. McCrone, 1991). Blast furnaces at Glengarnock closed in the 1930s and steel continued to be made in basic open hearth furnaces until the works closed (Charman, 1981; Gibson, 1956). Slag forms approximately a quarter of the overall lake shoreline. The lake water is circumneutral, with the volume of lake water assumed to dilute any influence on pH or trace element from interaction with the slag. The slag deposit has been largely capped with soil and been vegetated but where it is exposed on the lake shore (Fig. 1b), it typically has a hard top surface where the lake level has fluctuated. The slag surface has a mid-pale grey or cream colour (Fig. 1c), suggesting slag weathering and carbonation, likely facilitated by interaction with the loch water.

A sample of slag (sample RC18-02) was taken at 55.753359, −4.666098 and cut to make thin sections for scanning electron microscopy to investigate slag microstructure. The thin section was prepared using a Logitech PM6 lapping machine to prepare the glass slide and sample surface using silicon carbide 600 abrasive grit; sample and glass were bonded using Epothin epoxy resin at 30 °C for 2 h. A Petrothin was used to remove excess rock down to a thickness of ~100 μm before the lapping machine was used to get this down to 30 μm thickness. The section was polished using P2500 and P400 silicon carbide papers, followed by 3 μm, 1 μm and 0.3 μm aluminium oxide powder-water mixes.

The slag is dark grey in colour and porous, but all outer surfaces and many internal pore surfaces were coated in a cream-coloured material assumed to be calcite (Fig. 1c). A representative sample of ~1–2 g of this cream-coloured material was scraped off the outer surface of an off-cut of the slag sample using a steel blade and identified by powder X-Ray Diffraction (XRD) using a Rigaku MiniFlex 6G equipped with a D/teX Ultra detector, a 6-position (ASC-6) sample changer and Cu sealed tube (Kα1 and Kα2 wavelengths - 1.5406 and 1.5444 Å respectively). Phase identification was carried out with reference to the Crystallographic Open Database.

Values of $\delta^{13}C$ and $\delta^{18}O$ of the cream-coloured material coating the slag surface were obtained on 200 μg of powdered sample by CF-IRMS (continuous flow isotope ratio mass spectrometry) in the School of Geographical and Earth Sciences at the University of Glasgow. Powder was drilled from the surface and acidified using phosphoric acid (≥1.90 SG) and heated for 1nullh at 60 °C on an Elementar GasBench and analysed on a Isoprime 100 mass spectrometer. The sample was run in triplicate and the average reported as the result with 1 standard deviation. Values are calibrated to the Vienna PeeDee Belemnite (V-PDB) scale using NBS-18 and IAEA-603 reference standards. A secondary standard, IA-RO22 (Iso-Analytical Ltd.), was used to validate the calibration linearity for more depleted values of $\delta^{13}C$ and $\delta^{18}O$ than the reference standards have. Analytical uncertainties of 0.36‰ on $\delta^{13}C$ and 0.75‰ on $\delta^{18}O$ were obtained on measurements of IAEA-603 ($n = 20$) measured during the analytical batch (Table S1).

Sample imaging and chemical mapping was conducted on polished thin sections with a ~20 nm carbon coating using a Zeiss Sigma variable pressure field-emission-gun scanning electron microscope (VP-FEGSEM) equipped with an Oxford Instruments X-Max 80 mm^2 Silicon Drift Detector Energy dispersive detector, based in the Geoanalytical Electron Microscopy and Spectroscopy (GEMS) facility at the University of Glasgow. Backscattered Electron (BSE) imaging and Energy-dispersive X-ray spectroscopy (EDX) were conducted in high vacuum using high current mode and an accelerating voltage of 20 kV, working distance of 8.0 mm and aperture of 60 μm. EDX mapping data were acquired and processed using the Oxford Instrument AZtec software. All EDX maps shown have had the AZtec true map function applied, which removes background and artifacts, and resolves element peak overlap issues.

3. Results

Prior to microstructural analysis, the cream-coloured material was confirmed to be calcite using XRD analysis; the XRD spectra is shown in Fig. S1. Stable isotope analysis recorded $\delta^{13}C$ and $\delta^{18}O$ values of −18.50 ± 0.29‰ and −13.15 ± 0.49‰ respectively (Table S1). The microstructures created by partial carbonation of the slag are shown in Figs. 2–4, each highlighting the same textures in three different areas of the sample. SEM-BSE imaging shows 3 distinct compositional zones in the slag sample analysed (Fig. 2a, 3a and 4a). Fresh slag, i.e. that which has not reacted with CO_2, exhibits relatively bright areas and therefore more higher atomic number (metallic) elements. The fresh slag is not uniform in its appearance, with different mineral phases registering different greyscale values. The reacted slag has an overall darker appearance but with greyscale heterogeneity giving a 'speckly' appearance. The brighter patches are of similar greyscale values to the fresh slag and are likely to represent mineral phases which do not react with CO_2. The darker areas in between represent different mineral phases to that found in the fresh slag. The calcite (mineralised CO_2) is represented by areas of uniform grey colour between the pore space and reacted slag. Figs. 2a, 3a and 4a shows the clear spatial relationship between the three zones, with fresh slag and calcite always separated by a zone of reacted slag.

Corresponding EDX chemical mapping (Fig. 2b–d, 3b-d & 4b-d) shows the distribution of key elements between the different mineral phases in the fresh slag, reacted slag and calcite. There is higher concentration of Ca (Figs. 2b, 3b and 4b) in the fresh slag and the calcite than in the reacted slag. Si (Figs. 2c, 3c and 4c) is found in relatively even concentration in the fresh slag and reacted slag but not in the calcite. Fe (Figs. 2d, 3d and 4d) is heterogeneously distributed in the fresh slag and reacted slag but is not found in the calcite. In the fresh slag and reacted slag, Fe is found in higher concentration where there is no Ca and Si, indicating Fe-oxide; this corresponds with the brightest areas in the BSE imaging. In Fig. 3d, there is a suggestion that in Fe-rich crystals, the concentration of Fe is greater at the crystal edges than in the cores; this is corroborated by brighter greyscale values in the associated BSE image (Fig. 3a) at the edges of those crystals.

The EDX mapping in Figs. 2–4 shows the zone of reacted slag is typically ~250 μm diameter in this sample, although with some variation. A larger area of calcite has precipitated adjacent to a wider area of reacted slag in Fig. 2a, which is to be expected, with a greater volume of Ca being leached to facilitate calcite precipitation. However, the distribution of calcite on slag surfaces throughout the sample can be highly variable (Fig. 5). Some pores can be partly filled, completely filled, or have no calcite at all (Fig. 5a). The thickness of the calcite coating can vary over short distances, for example as shown in Fig. 5b where a thicker coating of calcite has formed in an area of slag with a larger crystal size than an adjacent area with a finer crystal size. In some regions, even on the outer surface of the slag which has the greatest exposure to atmospheric CO_2, there may be no calcite at all (Fig. 5c).

The morphology and texture of the precipitated calcite itself can also vary. The outer edge of the calcite deposit can be smooth or irregular, while the deposit can internally have relatively high porosity in some patches (Fig. 5d). In some instances, the calcite displays layering, parallel to the surface of the slag (Fig. 5e) indicating precipitation of layers

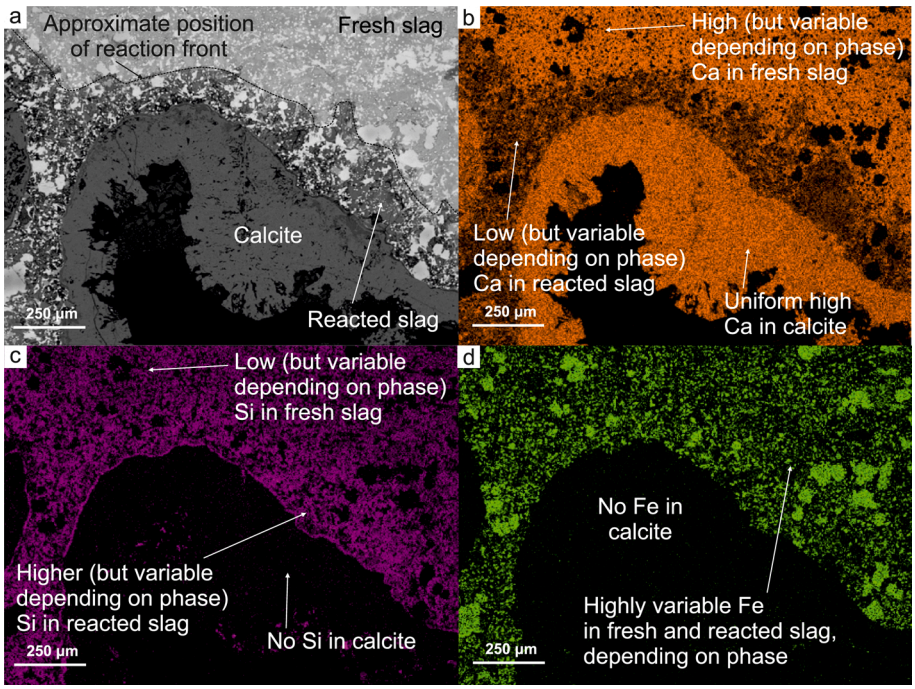

Fig. 2. scanning electron microscopy and chemical mapping of part of the slag sample; a) back-scattered electron image showing fresh slag, reacted slag and precipitated calcite; (b)–(d) electron dispersive X-ray element maps (Ca, Si and Fe, respectively) of the same area as (a) showing the presence of calcite (high Ca, no Si), fresh slag (mix of Ca, Fe and Si) and reacted slag (Si, Fe and low Ca).

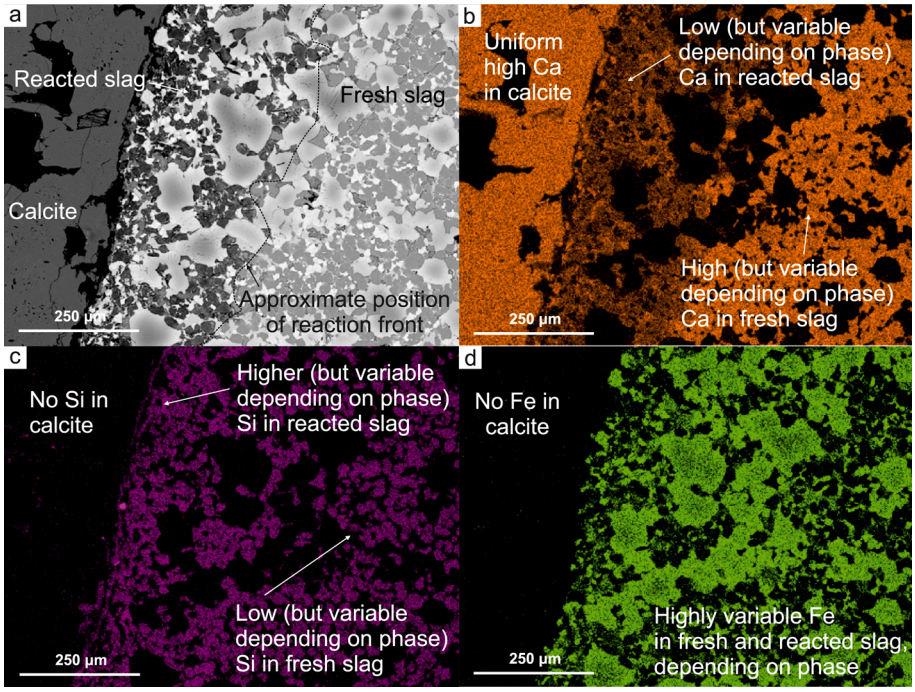

Fig. 3. scanning electron microscopy and chemical mapping of part of the slag sample; a) back-scattered electron image showing fresh slag, reacted slag and precipitated calcite; (b)–(d) electron dispersive X-ray element maps (Ca, Si and Fe, respectively) of the same area as (a) showing the presence of calcite (high Ca, no Si), fresh slag (mix of Ca, Fe and Si) and reacted slag (Si, Fe and low Ca).

over time. Calcite crystal shape within the deposits is often difficult to resolve with BSE and EDX but in some places, needle-shaped crystals can be observed; these may be growing at a different angle (Fig. 4a) or out into the pore perpendicular to the slag surface (Fig. 5e) or at a different angle (Fig. 4a).

4. Discussion

4.1. Nature and mechanism of carbonation

The distribution of mineral phases and major elements visible in the BSE imaging and EDX mapping respectively shows that CO_2 has reacted with slag and mineralised as calcite. When fresh out of the steelmaking

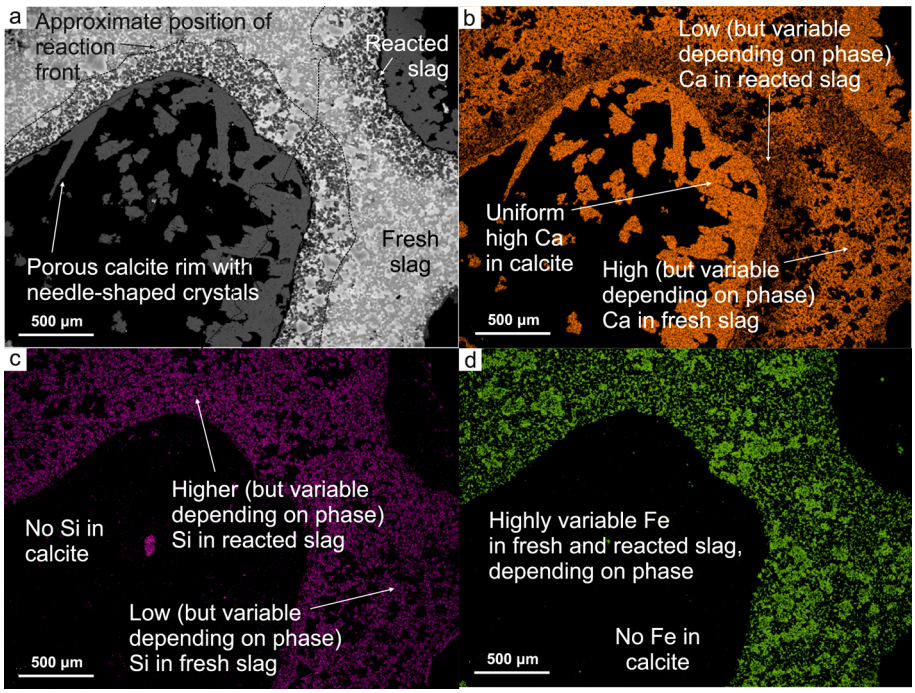

Fig. 4. scanning electron microscopy and chemical mapping of part of the slag sample; a) back-scattered electron image showing fresh slag, reacted slag and precipitated calcite; (b)–(d) electron dispersive X-ray element maps (Ca, Si and Fe, respectively) of the same area as (a) showing the presence of calcite (high Ca, no Si), fresh slag (mix of Ca, Fe and Si) and reacted slag (Si, Fe and low Ca).

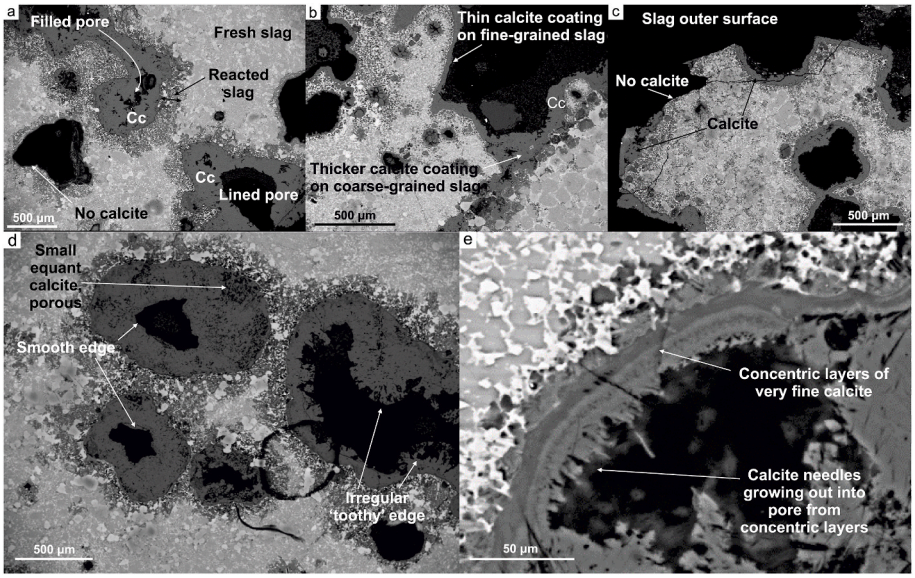

Fig. 5. back-scattered electron images showing different microstructural textures in the slag sample; a) in a small area, pores can be filled with calcite, lined with calcite, or have no calcite at all; (b) thickness of calcite coating on outer slag surface is variable, with a thicker coating at an area where the slag crystal size is larger; (c) some parts of the slag outer surface have no precipitated calcite; (d) the surface of the precipitated calcite can be smooth or jagged and irregular, while some domains of calcite are relatively porous; (e) layering in the calcite deposit parallel to the slag surface, with small needle-shaped calcite crystals growing out into the pore space.

furnace, pieces of slag will broadly have had high Ca throughout (Piatak et al., 2015). However, in this sample of legacy slag, there is now a zone of slag with lower Ca concentration on the outer surfaces and pore surfaces (Fig. 2a&b, 3a&b, 4a&b). This zone of lower Ca concentration represents slag which has undergone chemical reaction resulting in leaching of Ca (equation (1)). EDX mapping shows the relative concentration of Si and Fe remain unchanged between this zone and the 'fresh' slag, indicating leaching of specifically Ca rather than wholesale chemical change. In the sample analysed here, this zone of Ca leaching can be anything from 0 to 250 µm wide. Hobson et al. (2017) observed a similar narrow zone of low Ca on the outer surface of a BOF slag sample in their vanadium leaching study.

This leaching of Ca from slag is facilitated by reaction with water (equation (1)). The sample was taken from the surface of the slag deposit and so rainwater was a likely participant in the reaction. The uneven surface of the slag will have facilitated ponding or thin films of water to develop on the slag surface. Similarly, being adjacent to the lake (Fig. 1b) suggests lake water may also have facilitated Ca leaching via equation (1). While the lake level was below the level of the sampling location at the time of sampling (and during any other field visits), it is possible that elevated lake levels following heavy rainfall may have submerged the sample location for short periods, allowing lake water to promote Ca leaching.

As well as Ca, equation (1) also produces OH^- anions, resulting in a rise in pH. Mayes et al. (2018) documented this in the Howden Burn, a stream draining a slag heap at Consett in NE England. Even in a

relatively dilute setting such as a stream, the pH was greater than 11. In a thin film of moisture or millimetre-scale ponding of rainwater or lakewater on slag, the production of OH^- anions will therefore result in hyperalkalinity of that water. This hyperalkalinity promotes ingassing and hydroxylation of atmospheric CO_2 (equation (2)). The hydroxylated CO_2 then reacts with the dissolved Ca (leached from the slag) to precipitate calcite (equation (3)). The composition of the white material on the surfaces of sample RC18-02 in this study is confirmed as calcite by the XRD spectrum (Fig. S1). This mechanism of calcite precipitation has been documented in natural systems, where instead of slag the starting material is ultramafic rock, e.g. in the Semail ophiolite in Oman (Clark et al., 1992). This process of slag dissolution, CO_2 ingassing and hydroxylation, and calcite precipitation has also been documented in the ex-situ but slag-derived calcite tufa deposit at Consett (Mayes et al., 2018; Renforth et al., 2009). The SEM imaging and chemical mapping presented here (Figs. 2–5) shows that this same process also leads to in-situ carbonation, i.e. precipitation of calcite directly onto slag surfaces.

Measurement of carbon isotopes ($\delta^{13}C$) in the calcite can be used to fingerprint the source of the CO_2 for calcite precipitation. In hyperalkaline settings, such as at Consett and Oman described above, the source of CO_2 is interpreted to be atmospheric, with CO_2 ingassing and hydroxylation leading to precipitation due to the hyperalkalinity of the water. In the hyperalkaline springs in Oman, Falk et al. (2016) recorded $\delta^{13}C$ values from ~-25‰ to ~ -5‰ (Fig. 6). This range of values reflected the quite variable morphology of the stream bed and carbonate precipitate morphology (e.g. travertines and bottom floc), which resulted in a range of processes such as dissolved inorganic carbon (DIC) equilibration and recrystallisation. Pure end member hydroxylation would give a $\delta^{13}C$ value of ~ -25 to −27‰ (Dietzel et al., 1992; Falk et al., 2016; Renforth et al., 2009) with these other processes driving $\delta^{13}C$ closer to 0‰. In the tufa at Consett (Fig. 6), $\delta^{13}C$ values indicated mixing between hydroxylation and biogenic carbon inputs (with an end member of ~ -8‰ (Cerling, 1984)), reflecting the fact that calcite precipitation occurs away from the source of the Ca in a stream with ample scope for introduction of biogenic carbon (Renforth et al., 2009). In our sample from Glengarnock, where calcite precipitation is in-situ on the slag itself, there is limited scope for input of biogenic carbon. The $\delta^{13}C$ and $\delta^{18}O$ values of −18.38 ± 0.29‰ and −13.24 ± 0.49‰ respectively plot in the DIC equilibration field of Falk et al. (2016) (Fig. 6). This indicates that CO_2 was initially ingassed from the atmosphere and hydroxylated but underwent partial DIC equilibration (Fig. 6), driving the isotopic values partially towards 0‰ but precipitation will have occurred rapidly before full equilibration could occur.

The slag carbonation reaction is summarised in the conceptual model in Fig. 7. Certain phases in 'fresh' unreacted slag come into contact with water facilitating slag breakdown. In the hyperalkaline water on the slag surface, ingassed and hydroxylated CO_2 reacts with leached Ca to precipitate calcite. This leaves a buffer zone of reacted slag between fresh slag and newly precipitated calcite (Fig. 7).

4.2. Microstructures

The carbonation process has resulted in distinctive microstructures. Following the mechanisms outlined in Fig. 7, precipitated calcite is never observed in contact with 'fresh' (i.e. Ca-rich) slag – there is always a Ca-poor buffer zone of 'reacted' slag between them. Occasionally fresh slag is in contact with pore space or even the outer surface of the slag piece; in these locations no leaching of Ca from the slag and therefore no calcite has been precipitated. Some pores do not have any calcite lining them and have no reacted slag at the surface (Fig. 5a). Adjacent pores, however, are lined, or indeed almost filled with calcite. Instances such as this would suggest that the pore with no calcite was simply not connected to an external surface and therefore the slag surface around this pore did not react with CO_2 and water to precipitate calcite. Given the two-dimensional nature of this dataset, it is impossible to conclusively test this hypothesis here. X-Ray Computed Tomography (XCT) could be used to investigate pore connectivity (Khudhur et al., 2022b) although the attenuation coefficients of calcite and the various slag minerals are too close to clearly show the microstructures visible in the BSE imaging dataset in this study. Pore connectivity (or lack thereof) would be an obvious explanation for why some parts of the slag surface area have not reacted and precipitated calcite. However, a lack of access to air and water cannot be the only factor which controls whether slag carbonation occurs. Some parts of the outer surface of the slag sample have not reacted and do not have calcite precipitated on them (Fig. 5c) while the thickness of precipitated calcite varies greatly, both on external surfaces and internal pores (Figs. 2–5). This would suggest that it is not solely external environmental parameters, i.e. contact with CO_2 and water, which drive slag carbonation. The variation in microstructures produced suggest the possibility that there may be internal factors, i.e. physical and/or chemical properties of the slag itself, which influence the extent

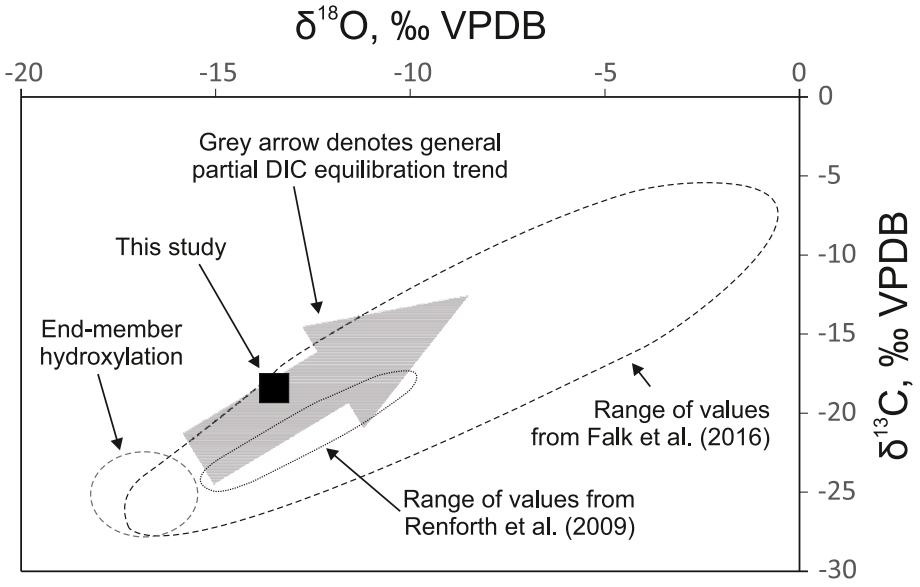

Fig. 6. $\delta^{13}C$ and $\delta^{18}O$ values from this study (black square) placed in the context of data from analogous studies (Renforth et al., 2009; Falk et al., 2016); end-member hydroxylation and partial DIC equilibration trend fields from Falk et al. (2016).

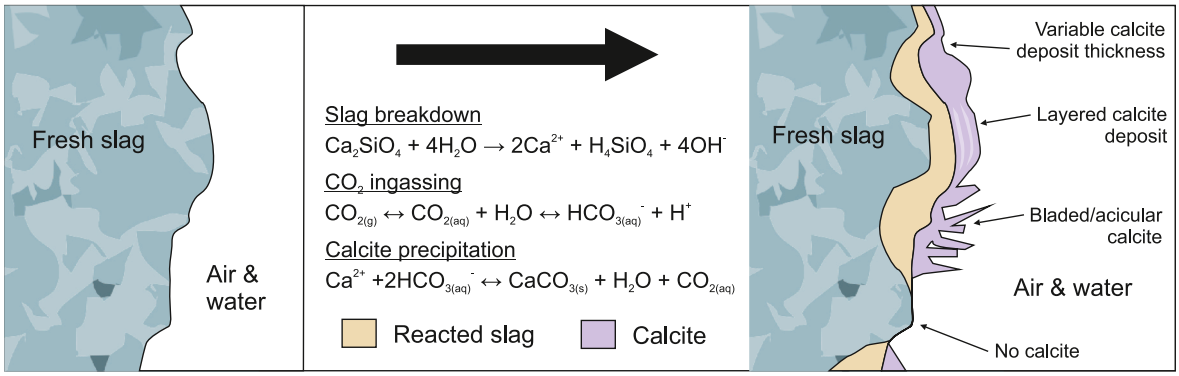

Fig. 7. conceptual model highlighting the slag carbonation process; fresh slag reacts with water resulting in a zone of reacted slag which is low in Ca at the slag surface, onto which calcite (comprising the leached Ca and ingassed and hydroxylated atmospheric CO_2) grows.

and distribution of slag carbonation and the resulting microstructures.

The microstructures of the slag and calcite can indicate whether physical and/or chemical properties of the slag influence the extent and distribution of carbonation and the resulting microstructures. Where calcite has precipitated, it covers an area of the thin section broadly proportional to the area of adjacent reacted slag perpendicularly across the slag surface. The reaction front between fresh slag and reacted slag is somewhat irregular and in places where the area of reacted slag is greater, the concurrent area of precipitated calcite is greater, for example in the pore in Fig. 2. BSE imaging clearly shows different mineral phases in the slag (e.g. Fig. 5). The brightest phases are present in both fresh and reacted slag and so do not appear to participate in the carbonation reaction. This is confirmed by EDX mapping which shows they are dominated by Fe with no Ca (e.g. Fig. 2d & 3d). It is the slightly darker phase (but still light grey in BSE, e.g. Fig. 2a) high in Ca (Fig. 2b) which is present in the fresh slag but absent in the reacted slag. This phase is likely to be a calcium silicate such as larnite (e.g. Mayes et al., 2018; Pullin et al., 2019). The proportion of this phase (and the Ca-poor phase that has replaced it in the reacted slag) relative to the Fe-rich phase which does not participate in the carbonation process does not vary greatly in the areas imaged in Figs. 2–5. As a result it is not immediately clear from this dataset that more extensive calcite deposits correspond with areas of slag which had higher proportions of Ca-rich mineral phases. However, the two-dimensional nature of this analysis means that these preliminary interpretations must be treated with caution and require further investigation, ideally in three dimensions.

Additionally, a variety of crystal morphologies of the precipitated calcite can be observed (Fig. 4a; Fig. 5d&e). In general, the precipitated calcite appears to be accumulation of microcrystalline calcite forming structureless, or occasionally layered (Fig. 5e), deposits on slag surfaces. Microcrystalline calcite has been documented in other settings where precipitation has occurred on nucleating surfaces at ambient conditions. For example, Liu et al. (2022) used secondary electron imaging to show that calcite precipitated in a similar mechanism on the surface of hydrated cement (carbonation of C–S–H) had a microcrystalline morphology. BSE imaging shows that accumulations of microcrystalline calcite on the slag surfaces are often porous, and this is also indicated in the imaging in the study of Liu et al. (2022). Occasional bladed/acicular calcite crystal morphologies were documented on the slag surfaces, growing into internal pores (Fig. 4a and 5e). Bladed crystal aggregates were documented by Bastianini et al. (2022) in an analogous ex-situ carbonate deposit derived from slag breakdown, including in relatively slow-moving water bodies not wholly dissimilar to that studied here. Bladed calcite is often documented at higher temperature settings, such as in geothermal and hydrothermal systems (e.g. Lu et al., 2018). In high-temperature systems, the reaction kinetics facilitated by the higher temperature allows larger bladed crystals to grow. The relatively static, but low temperature, environment of a fluid-filled pore within the slag may have allowed time for the occasional larger bladed/acicular crystal to grow, as well as the dominant microcrystalline calcite form.

4.3. *Impacts on slag valorisation*

The slag sample analysed in this study documents 'natural' atmospheric CO_2 mineralisation with slag at ambient conditions. Moreover, the carbon isotope data and detailed SEM imaging and chemical mapping show that atmospheric CO_2 can be passively mineralised in-situ, i.e. directly onto slag surfaces. While enhanced carbonation experiments have focused on leaching the Ca from slag and reacting it ex-situ with CO_2, such a pathway is energy- (and therefore CO_2-) intensive (Huijgen et al., 2007). There is a scope for in-situ passive carbonation of steel slag as a method for CO_2 capture, with design solutions and waste management practices that aim to enhance the CO_2 mineralisation in slag. Such solutions include enhancing the watering frequency of slag or sparging flue gas - which contains a higher CO_2 concentration than air - through the heap to increase the availability of CO_2 and H_2O which result in increasing the CO_2 uptake (Khudhur et al., 2022a; Roadcap et al., 2005).

CO_2 mineralisation can enhance valorisation of slag since it produces calcium carbonate and silica. This makes carbonated slag valuable supplementary cementitious material since these compounds are reactive during cement hydration (Liu et al., 2021). Additionally, calcium carbonate is economically valuable. In 2018, around 9.8×10^{10} kg of calcium carbonate was produced as this chemical is used in several industries, such as food, construction and pharmaceutical industries (Chang et al., 2017; Eloneva et al., 2008a). Recovering the precipitated carbonates and some elements that resides within alkaline wastes can enhance passive carbonation economics (Gomes et al., 2016). Optimising conditions for calcite precipitation can also enhance the economics of the steelmaking industry, since such optimisation reduces the net CO_2 released per tonne of steel produced therefore reducing the cost of carbon associated with this industry. Nevertheless, slag carbonation is associated with pH reduction which may result in enhancing the mobility of ecotoxic metals such as Cr and V. Lab-based leaching tests demonstrated that reduction of pH was associated with increase in V and Cr concentrations (Santos et al., 2012, van Zomeren et al., 2011). However, Hobson et al. (2017) demonstrated that in heap leaching, V release was affected by formation of secondary Ca–Si–H and $CaCO_3$ phases, and that $Ca_3(VO_4)_2$ equilibrium affected the concentration of V in leachate. Therefore, the dissolution of phases such as portlandite resulted in elevated Ca concentration, thereby reducing V concentration. However, when Ca was consumed during calcite precipitation, high release of V occurred. Leachates from different sites shows V concentrations above the environment quality standards (Mayes et al., 2008). Consequently, proposed large scale solutions should consider monitoring and controlling the leachates, possibly by using impermeable barrier technology as described elsewhere (Power et al., 2010).

5. Conclusions

SEM imaging and chemical mapping of legacy slag shows that atmospheric CO_2 mineralises directly on the surface of slag. A slag sample collected from a legacy slag heap at the site of the former Glengarnock Steelworks, Scotland, had a coating of calcite (confirmed by XRD analysis) in contact with a narrow zone of reacted slag. EDX chemical mapping showed this reacted slag to be depleted in Ca relative to the rest of the slag sample, indicating Ca had been leached through reaction with rainwater or the adjacent lake. Atmospheric CO_2 ingassed into the water film on the slag surfaces and hydroxylated before reacting with the Ca leached from the slag to precipitate calcite. Precipitated calcite crystal morphologies vary, ranging from bladed and acicular crystals to layered deposits of micron-scale equant crystals. Variable morphology and extent of calcite precipitation suggest a combination of internal (i.e. microstructural properties of the slag itself) and external (environmental conditions) factors result in the variable extent and distribution of passive carbonation documented.

The results here show that there is potential for in-situ CO_2 mineralisation with slag i.e. calcite precipitated directly onto the slag surface. This has implications for how new, and legacy, slag heaps are designed and managed so that atmospheric CO_2 can be drawn down and mineralised 'naturally' by the slag at ambient conditions as part of the slag valorisation and reutilisation process.

Declaration of competing interest

The authors declare that they have no known competing financial interests or personal relationships that could have appeared to influence the work reported in this paper.

Data availability

Data will be made available on request.

Acknowledgements

Associate Editor Thomas Gimmi, and two anonymous reviewers, are thanked for their comments which considerably improved this manuscript.

This research did not receive any specific grant from funding agencies in the public, commercial, or not-for-profit sectors.

Appendix A. Supplementary data

Supplementary data to this article can be found online at https://doi.org/10.1016/j.apgeochem.2023.105649.

References

Baciocchi, R., Costa, G., Polettini, A., Pomi, R., 2009. Influence of particle size on the carbonation of stainless steel slag for CO2 storage. Greenhouse Gas Control Techn. 9 1, 4859–4866.
Bastianini, L., Rogerson, M., Mercedes-Martín, R., Prior, T.J., Mayes, W.M., 2022. What are the different styles of calcite precipitation within a hyperalkaline leachate? A sedimentological Anthropocene case study. Deposit. Record 8, 355–381.
Cerling, T.E., 1984. The stable isotopic composition of modern soil carbonate and its relationship to climate. Earth Planet Sc. Lett. 71, 229–240.
Chang, E.E., Chiu, A.-C., Pan, S.-Y., Chen, Y.-H., Tan, C.-S., Chiang, P.-C., 2013. Carbonation of basic oxygen furnace slag with metalworking wastewater in a slurry reactor. Int. J. Greenh. Gas. Con. 12, 382–389.
Chang, E.E., Pan, S.-Y., Chen, Y.-H., Tan, C.-S., Chiang, P.-C., 2012. Accelerated carbonation of steelmaking slags in a high-gravity rotating packed bed. J. Hazard Mater. 227–228, 97–106.
Chang, R., Kim, S., Lee, S., Choi, S., Kim, M., Park, Y., 2017. Calcium carbonate precipitation for CO2 storage and utilization: a review of the carbonate crystallization and polymorphism. Front. Energy Res. 5.
Charman, D., 1981. Glengarnock, a Scottish Open Hearth Steelworks: the Works, the People: a Report on the Manpower Services Commission Conservation Projects Carried Out at Glengarnock, Ayrshire, pp. 1979–1980.
Clark, I.D., Fontes, J.-C., Fritz, P., 1992. Stable isotope disequilibria in travertine from high pH waters: laboratory investigations and field observations from Oman. Geochem. Cosmochim. Acta 56, 2041–2050.
Dietzel, M., Usdowski, E., Hoefs, J., 1992. Chemical and 13C/12C- and 18O/16O-isotope evolution of alkaline drainage waters and the precipitation of calcite. Appl. Geochem. 7, 177–184.
Eloneva, S., Teir, S., Salminen, J., Fogelholm, C.-J., Zevenhoven, R., 2008a. Fixation of CO2 by carbonating calcium derived from blast furnace slag. Energy 33, 1461–1467.
Eloneva, S., Teir, S., Salminen, J., Fogelholm, C.-J., Zevenhoven, R., 2008b. Steel converter slag as a raw material for precipitation of pure calcium carbonate. Ind. Eng. Chem. Res. 47, 7104–7111.
Falk, E.S., Guo, W., Paukert, A.N., Matter, J.M., Mervine, E.M., Kelemen, P.B., 2016. Controls on the stable isotope compositions of travertine from hyperalkaline springs in Oman: insights from clumped isotope measurements. Geochem. Cosmochim. Acta 192, 1–28.
Gibson, J., 1956. Basic open heath steelmaking- cold metal practice. J. West Scotland Iron and Steel Institute 63, 65–90.
Gomes, H.I., Mayes, W.M., Rogerson, M., Stewart, D.I., Burke, I.T., 2016. Alkaline residues and the environment: a review of impacts, management practices and opportunities. J. Clean. Prod. 112, 3571–3582.
Guo, J., Bao, Y., Wang, M., 2018. Steel slag in China: treatment, recycling, and management. Waste Manage. (Tucson, Ariz.) 78, 318–330.
Hobson, A.J., Stewart, D.I., Bray, A.W., Mortimer, R.J.G., Mayes, W.M., Rogerson, M., Burke, I.T., 2017. Mechanism of vanadium leaching during surface weathering of basic oxygen furnace steel slag blocks: a microfocus X-ray absorption spectroscopy and electron microscopy study. Environ. Sci. Technol. 51, 7823–7830.
Huijgen, W.J.J., Comans, R.N.J., Witkamp, G.J., 2007. Cost evaluation of CO2 sequestration by aqueous mineral carbonation. Energy Convers. Manag. 48, 1923–1935.
Huijgen, W.J.J., Witkamp, G.J., Comans, R.N.J., 2005. Mineral CO2 sequestration by steel slag carbonation. Environ. Sci. Technol. 39, 9676–9682.
Khudhur, F.W.K., MacDonald, J.M., Macente, A., Daly, L., 2022a. The utilization of alkaline wastes in passive carbon capture and sequestration: promises, challenges and environmental aspects. Sci. Total Environ. 823, 153553.
Khudhur, F.W.K., Macente, A., MacDonald, J.M., Daly, L., 2022b. Image-based analysis of weathered slag for calculation of transport properties and passive carbon capture. Microsc. Microanal. 1–12.
Kirchofer, A., Becker, A., Brandt, A., Wilcox, J., 2013. CO2 mitigation potential of mineral carbonation with industrial alkalinity sources in the United States. Environ. Sci. Technol. 47, 7548–7554.
Liu, G., Schollbach, K., Li, P., Brouwers, H.J.H., 2021. Valorization of converter steel slag into eco-friendly ultra-high performance concrete by ambient CO2 pre-treatment. Construct. Build. Mater. 280, 122580.
Liu, X., Feng, P., Cai, Y., Yu, X., Yu, C., Ran, Q., 2022. Carbonation behavior of calcium silicate hydrate (C-S-H): its potential for CO2 capture. Chem. Eng. J. 431, 134243.
Lu, Y.-C., Song, S.-R., Taguchi, S., Wang, P.-L., Yeh, E.-C., Lin, Y.-J., MacDonald, J., John, C.M., 2018. Evolution of hot fluids in the Chingshui geothermal field inferred from crystal morphology and geochemical vein data. Geothermics 74, 305–318.
Mayes, W.M., Riley, A.L., Gomes, H.I., Brabham, P., Hamlyn, J., Pullin, H., Renforth, P., 2018. Atmospheric CO2 sequestration in iron and steel slag: Consett, county durham, United Kingdom. Environ. Sci. Technol. 52, 7892–7900.
Mayes, W.M., Younger, P.L., Aumonier, J., 2008. Hydrogeochemistry of alkaline steel slag leachates in the UK. Water, Air, Soil Pollut. 195, 35–50.
McCrone, G., 1991. Urban renewal: the scottish experience. Urban Stud. 28, 919–938.
Netinger Grubeša, I., Barišić, I., Fucic, A., Bansode, S.S., 2016. 4 - application of blast furnace slag in civil engineering: worldwide studies. In: Netinger Grubeša, I., Barišić, I., Fucic, A., Bansode, S.S. (Eds.), Characteristics and Uses of Steel Slag in Building Construction. Woodhead Publishing, pp. 51–66.
Piatak, N.M., Parsons, M.B., Seal, R.R., 2015. Characteristics and environmental aspects of slag: a review. Appl. Geochem. 57, 236–266.
Power, I.M., Dipple, G.M., Southam, G., 2010. Bioleaching of ultramafic tailings by acidithiobacillus spp. for CO2 sequestration. Environ. Sci. Technol. 44, 456–462.
Pullin, H., Bray, A.W., Burke, I.T., Muir, D.D., Sapsford, D.J., Mayes, W.M., Renforth, P., 2019. Atmospheric carbon capture performance of legacy iron and steel waste. Environ. Sci. Technol. 53, 9502–9511.
Renforth, P., 2019. The negative emission potential of alkaline materials. Nat. Commun. 10, 1401.
Renforth, P., Manning, D.A.C., Lopez-Capel, E., 2009. Carbonate precipitation in artificial soils as a sink for atmospheric carbon dioxide. Appl. Geochem. 24, 1757–1764.
Riley, A.L., MacDonald, J.M., Burke, I.T., Renforth, P., Jarvis, A.P., Hudson-Edwards, K. A., McKie, J., Mayes, W.M., 2020. Legacy iron and steel wastes in the UK: extent, resource potential, and management futures. J. Geochem. Explor. 219, 106630.
Roadcap, G.S., Kelly, W.R., Bethke, C.M., 2005. Geochemistry of extremely alkaline (pH > 12) ground water in slag-fill aquifers. Ground Water 43, 806–816.
Salman, M., Cizer, Ö., Pontikes, Y., Santos, R.M., Snellings, R., Vandewalle, L., Blanpain, B., Van Balen, K., 2014. Effect of accelerated carbonation on AOD stainless steel slag for its valorisation as a CO2-sequestering construction material. Chem. Eng. J. 246, 39–52.
Santos, R.M., Ling, D., Sarvaramini, A., Guo, M., Elsen, J., Larachi, F., Beaudoin, G., Blanpain, B., Van Gerven, T., 2012. Stabilization of basic oxygen furnace slag by hot-stage carbonation treatment. Chem. Eng. J. 203, 239–250.
Santos, R.M., Van Bouwel, J., Vandevelde, E., Mertens, G., Elsen, J., Van Gerven, T., 2013. Accelerated mineral carbonation of stainless steel slags for CO2 storage and waste valorization: effect of process parameters on geochemical properties. Int. J. Greenh. Gas. Con. 17, 32–45.

USGS, 2018. USGS Minerals Yearbook.
van Zomeren, A., van der Laan, S.R., Kobesen, H.B.A., Huijgen, W.J.J., Comans, R.N.J., 2011. Changes in mineralogical and leaching properties of converter steel slag resulting from accelerated carbonation at low CO2 pressure. Waste Manage. (Tucson, Ariz.) 31, 2236–2244.
Yu, J., Wang, K., 2011. Study on characteristics of steel slag for CO2 capture. Energy Fuel. 25, 5483–5492.